Local, single-molecule oxidative cleaving of DNA origami by C_{60} on an AFM tip

A. Ray[1], C. Passiu[2], S. N. Ramakrishna[2], A. Rossi[2, 3], A. Kuzuya[4], N. D. Spencer[2], Y. Yamakoshi[1]*

[1]Laboratorium für Organische Chemie, ETH Zürich, Vladimir-Prelog-Weg 3, CH-8093 Zürich, Switzerland.

[2]Laboratory for Surface Science and Technology, Department of Materials, ETH Zurich, Vladimir-Prelog-Weg 5, CH-8093 Zürich, Switzerland.

[3]Dipartimento di Scienze Chimiche e Geologiche, Università degli Studi di Cagliari, Cittadella Universitaria di Monserrato, I – 09100 Cagliari, Italy

[4]Department of Chemistry and Materials Engineering, Kansai University, Yamate-cho 3-3-35, Suita, 564-8680 Osaka, Japan.

*yamakoshi@org.chem.ethz.ch

Abstract: Spatially controlled single-molecule oxidation of DNA was performed by photocatalytic generation of singlet oxygen on chemically functionalized AFM tips. A waffle-type DNA origami deposited on a mica surface is site-specifically destroyed by generation of reactive oxygen species at the AFM tip, which was modified with a C_{60}-tripod photocatalyst. Upon AFM scanning under photoirradiation, DNA morphology changes, corresponding to oxidative damage, were clearly observed at the single-molecule level. The DNA cleavage occurred with strict dependence on photoirradiation and the presence of C_{60} on the AFM tip.

With the advent of scanning probe microscopies (SPMs) and electron microscopies (EMs), it has become possible to visualize and analyze single molecules(*1*). These microscope technologies have enabled detailed structural analysis of substrate molecules with sub-nm resolution, as well as providing time-dependent dynamic measurements of single molecules, independently of other molecules. An early example of scanning tunneling microscopy (STM) imaging detected the motion of a single organic molecule (molecular motor) on the surface(*2*). Atomic force microscopy (AFM) imaging of transmembrane receptors was able to provide the different conformational changes of individual molecules in the system(*3*). Bond formation and cleavage could also be demonstrated on the surface at the single-molecule level(*4*). These data generally are not obtainable by traditional bulk studies, which provide only ensemble-averaged data of all molecules in the system.

AFM(*5*) with extremely sharp tips has become an important tool for the topological analysis of substrate surfaces, including the imaging of non-conductive and relatively large biomolecules, while their functions remain intact, under physiological hydrated conditions. By means of the attachment of suitable organic molecules onto tips, AFM can perform further structural interrogations. Chemical force microscopy (CFM)(*6*), one of the earliest examples, uses AFM tips functionalized with molecules to detect chemical species on the substrate surface by measuring the tip-sample interaction at the pN level. With this CFM technique, molecular recognition, such as ligand-receptor(*7, 8*) and antigen-antibody(*9*) interactions, as well as protein unfolding(*10-12*), chiral recognition(*13*), and supramolecular host-guest complexation(*14-16*) have been studied at a single-molecule level. In addition to direct structural and binding studies, single-molecule technologies are important for bottom-up manipulation techniques to construct nm-scale architectures

possessing new functions. AFM has been used to construct nanostructures by tip-based nanolithography and early studies include dip-pen nanolithography of nanostructured self-assembled monolayers (SAM) of alkanethiols on gold surfaces (*17*). Separately, tip-induced chemical reactions have been applied to the SAMs on surfaces using chemical species on an AFM tip. Such a tip, chemically functionalized with sulfonic acid was used for the acidic deprotection of the protected terminal alcohol groups on a SAM surface(*18*). Cu-coated AFM tips catalytically enabled click reactions on an azide-terminated SAM surface(*19*). The physical properties of an AFM tip, such as electrical bias and mechanical force, have also been used to induce both surface reduction/oxidation(*20*) and retrocycloaddition(*21*).

In this study, we have devised an AFM tip incorporating a photocatalyst for the spatially controlled oxidation of molecules adsorbed to a surface. As a robust, single-molecule photocatalyst, a C_{60}-derivative was used to generate $^1O_2$ under visible-light irradiation, allowing localized oxidative reaction of a substrate molecule on a mica surface. Tripod-C_{60} molecule **1** (Fig. 1) was designed to enable the stable attachment of a C_{60} molecule on an Au-coated AFM tip. The molecular design was carefully chosen to allow the C_{60} to be close to the substrate surface while maintaining sufficient distance from the Au-coated AFM probe, which could potentially quench photoexcited molecules(*22*) (Fig. 1a). A related tripod platform, based on Keana's original design (*23*), previously provided CFM data with high accuracy and reproducibility due to a broad scaffold structure with multiple S-Au bonds(*24*), which serve to anchor the single molecule tips onto the gold surfaces in a dispersed and immovable manner with an "upright" orientation, as observed by NC-AFM(*25, 26*).

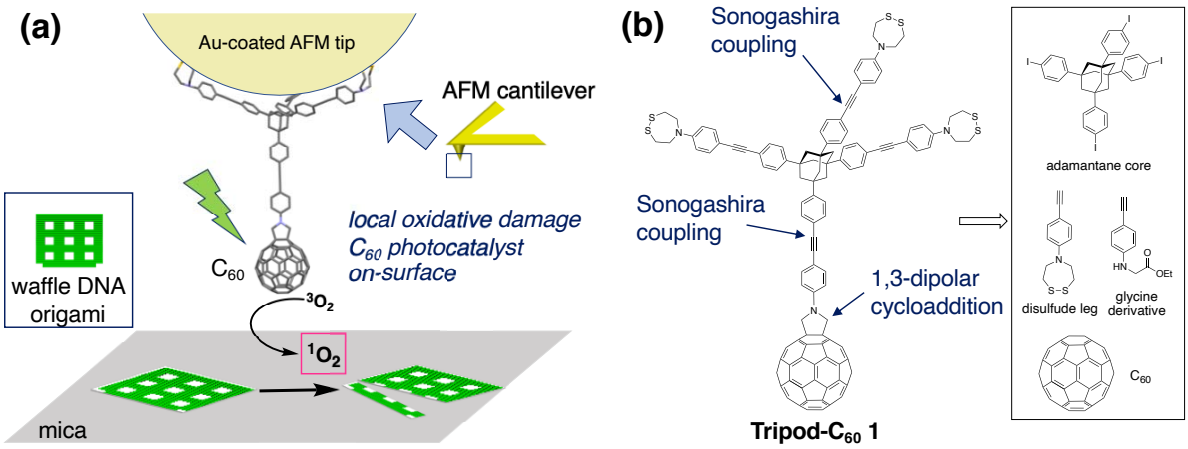

Fig. 1. Single-molecule oxidative damage of DNA on a surface by $^1O_2$ generated from a C_{60} photocatalyst on an AFM tip. (a) Schematic illustration of tripod-C_{60} **1** attached to a gold AFM tip and oxidative damage of substrate DNA origami by $^1O_2$ generated from photoexcited C_{60}. (b) Chemical structure and retrosynthesis of tripod-C_{60} **1**.

As substrates for single-molecule oxidation, in this study, we chose a waffle-type DNA origami for its flat and uniform morphology(*27*) to perform the oxidative damage (kirigami) on surface. Such DNA kirigami technique was reported using DNA strand displacement which was carried out in the solution phase(*28*). In our recent investigations, this waffle-shaped DNA origami was immobilized onto a mica surface in the presence of Mg^{2+} and its oxidative damage by C_{60}-PEG upon photoirradiation(*29*) was observed by

time-lapse AFM imaging in fluid. Tripod-C_{60} **1** was synthesized by a separate synthesis of each part (adamantane core, acetylene disulfide leg, and glycine linker), followed by their connection *via* Sonogashira coupling and 1,3-dipolar cycloaddition (Prato reaction) with C_{60} (Fig. 1b, Scheme S1). Compound **1** and all synthetic intermediates were purified and fully characterized by spectroscopic analysis (Figs. S1-21). For control experiments, a tripod molecule without C_{60} (tripod **2**) and a C_{60} derivative without the tripod-scaffold part (*N*-methylfulleropyrrolidine **3**) were synthesized, and subjected to the reaction with an Au surface for surface analysis and AFM imaging (Fig. 2a).

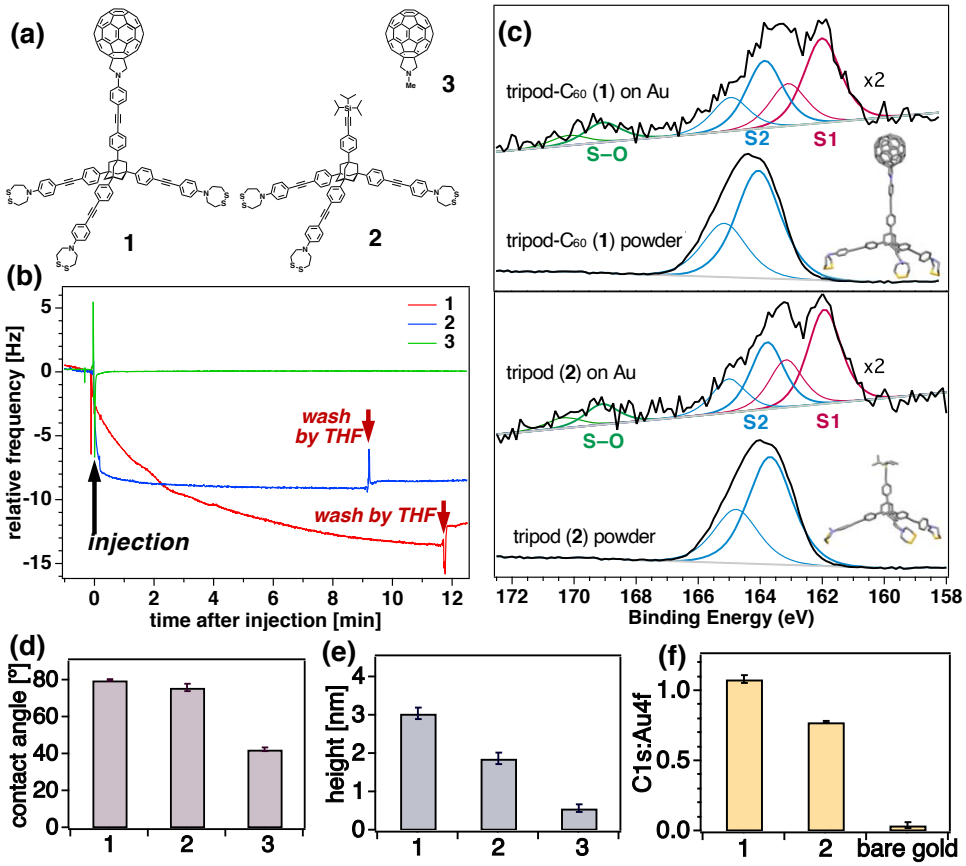

Fig. 2. Characterization of Au surfaces with compounds 1-3. (a) Structures of tripod-C_{60} **1**, tripod **2**, and *N*-methylfulleropyrrolidine **3** used for the Au surface functionalization. (b) QCM diagrams corresponding to the attachment of **1 – 3** onto the Au-coated sensors. The crystal was excited to oscillate at its resonant frequency. The changes in frequency were monitored upon injection of THF solutions of compounds **1** – **3**. (c) High-resolution XPS spectra of the S2p photoelectrons from the Au surface with chemisorbed (upper) or physiosorbed (lower) compounds **1** and **2**. (d) Contact angles of the Au surface treated with THF solutions of **1-3**. (e) Estimated height from ellipsometry data of the Au surface treated with THF solutions of **1-3**. (f) The peak ratios of C1s/Au4f obtained from XPS of gold surfaces with chemisorbed **1** and **2**. The peak intensity ratio of C1s/Au4f was obtained from the peak areas divided by the corrected photoionization cross sections (C1s = 1.52) and Au4f (32.23). The ratio is provided for gold surfaces with chemisorbed **1** and **2**. For the measurements of (c)-(f), the gold surfaces were prepared by Au-deposition onto a chromium-covered glass slide. Photoionisation cross sections were those published by J.H.Scofield(*30*) and were corrected for the matrix and the instrument geometry as reported(*31*).

Direct characterization of the functionalized, gold-coated AFM tip was not possible due to the limited surface area on the AFM tip apex; therefore, larger gold surfaces were used to investigate the reaction with tripod-C_{60} **1** or control compounds **2** and **3**. These were characterized by quartz crystal microbalance (QCM) analysis, X-ray photoelectron spectroscopy (XPS), static contact-angle determination, ellipsometry, and AFM measurements (Figs. 2-3). QCM was used to monitor the coverage of gold sensors with the attached molecules **1** - **3**. A solution of each compound **1** - **3** (0.1 mM in THF) was injected into a QCM sensor cell, which was initially stabilized in THF. As shown in Fig. 2b, a significant decrease in the frequency was observed upon injection of solutions of compound **1** or **2**, corresponding to mass changes upon the attachment of molecules. The frequency decrease plateaued at ca. 10 min after injection(*32*) and slightly increased upon surface rinsing by subsequent injection of THF. The decreases in frequency values, 11 and 7 Hz for **1** and **2**, respectively, showed a good correlation to the relative molecular weights of **1** (MW 2002.5) and **2** (MW 1318.1). From the Sauerbrey equation(*33*), the total masses adsorbed upon injection of compounds **1** and **2** were calculated to be 221 and 150 ng•cm^{-2}, respectively, indicating nearly full coverage of the Au surface with these molecules. In contrast, control experiment with compound **3** showed no significant change in the frequency (Fig. 2b), suggesting that the C_{60} moiety itself was not involved in the attachment of the molecules onto the gold surface. These results strongly suggest that tripod-C_{60} **1** and tripod **2** were immobilized onto an Au surface by the disulfide moieties, which selectively reacted with the Au surface to form covalent S-Au bonds, resulting in the desired orientation of molecules with the photosensitive C_{60} moiety atop the AFM tip apex(*34*).

To confirm the S-Au bond formation between the tripod and Au surface, XPS analyses were performed on the gold surfaces with tripods **1** and **2** (Fig. 2c). A gold substrate was prepared by vapor deposition onto the chromium layer, which was initially deposited onto freshly cleaned glass microscope slides(*35*). This Au surface was immersed into THF solution (0.1 mM) of compounds **1** or **2** overnight and then thoroughly washed with THF before analysis. For comparison experiments, Au surfaces with deposited dry powders of compounds **1** and **2** were used. The S2p region of XPS spectra (Fig. 2c) showed substantial changes in the surfaces when exposed to solutions of **1** and **2**, in comparison to the physisorbed controls. In the physisorbed control samples, only the S2 ($S2p_{3/2}$ + $S2p_{1/2}$) peak with an intensity maximum at 163.5 eV of binding energy was observed. The Au surfaces prepared with solutions of **1** and **2** revealed a new peak S1 ($S2p_{3/2}$ + $S2p_{1/2}$) with a maximum at 161.7 eV, clearly indicating the chemisorption of the molecules by the formation of S-Au bonds(*36*-*38*). While the S2p peaks observed on the Au surface with chemisorbed **1** and **2** may correspond to S-S bonds of physisorbed molecules, as the same peaks were observed in the powder samples of **1** and **2**, they may also be ascribed to the formation of sulfur species produced by X-ray damage (*39*), as the slight generation of oxidized sulfur (S-O) species were also detected as an artefact of radiation. The ratio of the peaks of S1, S2, and S-O in the S2p region were ca. 50, 39, and 11% for tripod **1** and 49, 40, and 11% for tripod **2**, respectively, clearly confirming the chemisorption of the molecules by the formation of covalent S-Au bonds, which enable the stable attachment of the tripod molecule to the gold surface. Furthermore, the peak ratios of C1s and Au4f for chemisorbed **1** and **2** were observed to be much higher than that of bare gold, supporting the efficient adsorption of carbon-based molecules onto the Au surface (Fig. 2f).

The Au surfaces treated with the solutions of **1**, **2**, and **3** were subjected to contact-angle and ellipsometry measurements. While the water contact angle of the surface with **3** showed ca. 42º, which lay within a range of reported values for template-stripped Au

surfaces (20 - 80º)(*40*), the surface with **1** and **2** showed significantly higher contact angle with ca. 80º and 76º, respectively, clearly indicating the immobilization of hydrophobic molecules (Fig. 2d). Ellipsometry analyses of the same Au surfaces with **1** and **2** revealed the thickness of the adsorbed layer to be 3.05 and 1.88 nm, respectively (Fig. 2e), in good agreement with the simulated heights of **1** and **2** (ca. 3.1 and 2.0 nm) in their upright forms.

In previous studies, similar tripod molecules were immobilized onto an Au surface in a dispersed manner(*25, 41*) so that they could act as molecular tips with utility for single-molecule studies. In this study, the chemisorption of the tripod-C_{60} **1** and tripod **2** were analyzed by AFM imaging. An ultra-flat Au surface, which was prepared by the template-stripping method(*42, 43*), was soaked in a 0.1 mM THF solution of **1** or **2** in the absence of light. To avoid full coverage of the molecule on the gold surface, this chemisorption process was performed over a short period (3 min) to obtain a dispersed adsorbed layer of the molecules(*41*). Subsequently, the surface was washed with THF, dried with N_2, and subjected to tapping-mode AFM imaging using a silicon cantilever (OMCL-AC160 TS, frequency: 300 kHz; spring constant: 26 $N \cdot m^{-1}$; tip radius: 7 nm). The resulting AFM images of chemisorbed **1** and **2** are shown in Fig. 3a-b. In both surfaces, the molecules were observed as small dots. In good agreement with the QCM results, which showed faster adsorption of the tripod **2** molecules, more molecules were observed on the compound-**2**-exposed surface (Fig. 3b). Histogram analyses determined the heights (Fig. 3c-e) of molecules **1** and **2** on the gold surface with means of 3.15 and 2.12 nm, respectively, in good correlation with their estimated molecular height (ca. 3.1 and 2.0 nm for **1** and **2**) when adsorbed in an upright fashion.

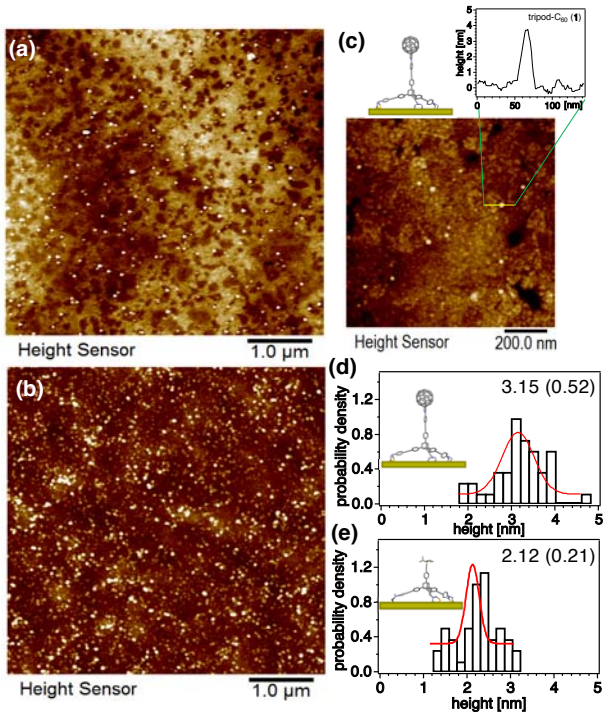

Fig. 3. AFM images of tripods 1 and 2 adsorbed onto an Au surface. (a-b) AFM images of tripod-C_{60} **1** (a) and tripod **2** (b) on Au. (c) Section analysis of representative AFM image of tripod-C_{60} **1**. (d-e) Histogram analysis of height of AFM images of **1** (d) and **2** (e). Template-stripped gold surfaces were used for the immobilization of compounds **1** and **2**.

Based on the results above, which confirmed the chemisorption of tripod molecules on the gold surface, tripod-C_{60} **1** was used for AFM tip functionalization. An Au-coated AFM tip (Bruker NPG-10, with nominal values of frequency: 65 kHz; spring constant: 0.35 $N•m^{-1}$; tip radius: 20 nm) was cleaned by UV/ozone treatment, picked up with a house-built Teflon cantilever holder, and soaked in a toluene solution (0.1 mM) of tripod-C_{60} **1**. Subsequently, the tip was thoroughly washed and mounted onto the AFM head. As a substrate for DNA manipulation, a waffle-type DNA origami with a relatively flat shape and a uniform and distinct morphology with 9-wells(*27*), was used. It was expected that this flat type of the DNA substrate would be relatively prone to oxidative damage by $^1O_2$, due to its large surface area, consistent with our previous results employing water-soluble fullerenes in the solution phase(*29*).

Using an AFM tip, functionalized with tripod-C_{60} **1**, continuous AFM imaging of DNA origami was carried out under photoirradiation at selected locations on the DNA substrate surface (835 x 835 nm), as illustrated in the inset of Fig. 4. A monochromatic light with a maximum wavelength of 532 nm was used for the photoirradiation, since no significant DNA damage can be caused by such visible light, while the C_{60} core can be excited. Interestingly, functionalization of the AFM tip with tripod-C_{60} did not cause a significant decrease in the resolution of AFM images of waffle DNA. AFM imaging with a smaller scan size (835 x 835 nm) was repeated continuously under photoirradiation over a total of 50 min (*step 1*, Fig, 4a-c). Time-dependent morphology changes of DNA origami could be observed in the scanned area. Afterward, the light was switched off and AFM imaging was performed over a larger scan size (1.8 x 1.8 μm, including smaller tip-treated area) (*step 2,* Fig. 4d). Significant damage to the waffle DNAs was observed only in the smaller area, where the AFM scanning were performed under photoirradiation using an AFM tip with tripod-C_{60} **1** (marked with red square), while less DNA damage was observed in the outer area. As a control experiment, scanning with an AFM tip functionalized with tripod **2** was performed on the waffle DNA origami substrate under photoirradiation. As shown in Fig. 4e-f, no DNA damage was observed after 40 min of scanning under photoirradiation, confirming that the photocatalyst C_{60} is essential for the oxidative damage of the DNA origami on the surface. DNA damage was not observed in the absence of light (Fig. S30), even when applying much higher force (150 - 200 pN, Fig. S31), confirming that DNA morphology changes were not caused by repeated scanning under harsh conditions(*44*)(*45*).

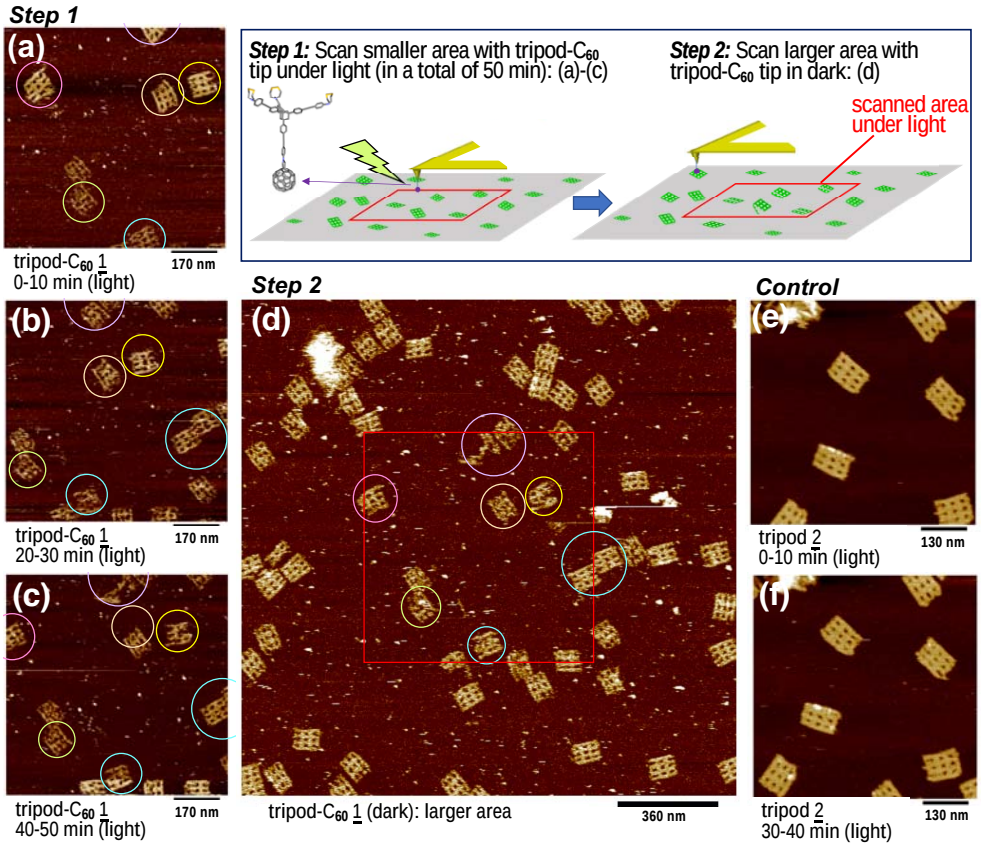

Fig. 4. AFM images of waffle-type DNA origami following tip reaction by tripod-C_{60} (1) AFM tip under photoirradiation. (a-c) AFM images of DNA origami in which a small area (835 x 835 nm) was scanned with tripod-C_{60} (**1**) tip under photoirradiation for 0 – 10 min (a), 20 – 30 min (b), and 40 – 50 min (c) (*step 1* in the inset). (d) AFM image of DNA origami scanned over a larger area (1.8 x 1.8 μm) after step 1 photoreaction (*step 2* in the inset). Imaging was performed in the dark with tripod-C_{60} (**1**) tip. The red square is the scanned area in the *step 1* photoreaction (not completely accurate due to the drift in the scanning). (e-f) AFM images of DNA origami in a smaller area (650 x 650 nm) scanned with tripod (**2**) tip under photoirradiation for 0 – 10 min (e) and 30 – 40 min (f). Photoirradiation was carried out using monochromatic light with a maximum wavelength of 532 nm.

Based on the results above, AFM tip-induced DNA damage was shown to have occurred at the single-molecule level. Fig. 5 shows the result of DNA damage of only two molecules **A** and **B**, while intact DNA **C** was observed nearby, outside the scanned area. After initial imaging of intact DNA under dark condition (Figs. 5a and S32a), the smaller area, where DNA **A** and **B** were located (red square area), were scanned continuously with photoirradiation. Time-dependent morphology changes of waffle DNA **A** and **B** were clearly observed, as shown in Fig. 5c-e (and Fig. S32d-h). Importantly, the DNA **C** located outside the scanned area was observed by AFM imaging (Fig. 5b) to be intact after photoirradiation. Single-molecule morphology analyses of the DNA origami **A**-**C** (Fig. 5f) showed a significant decrease in the height of treated DNA **A** and **B**, while control DNA **C** remained intact.

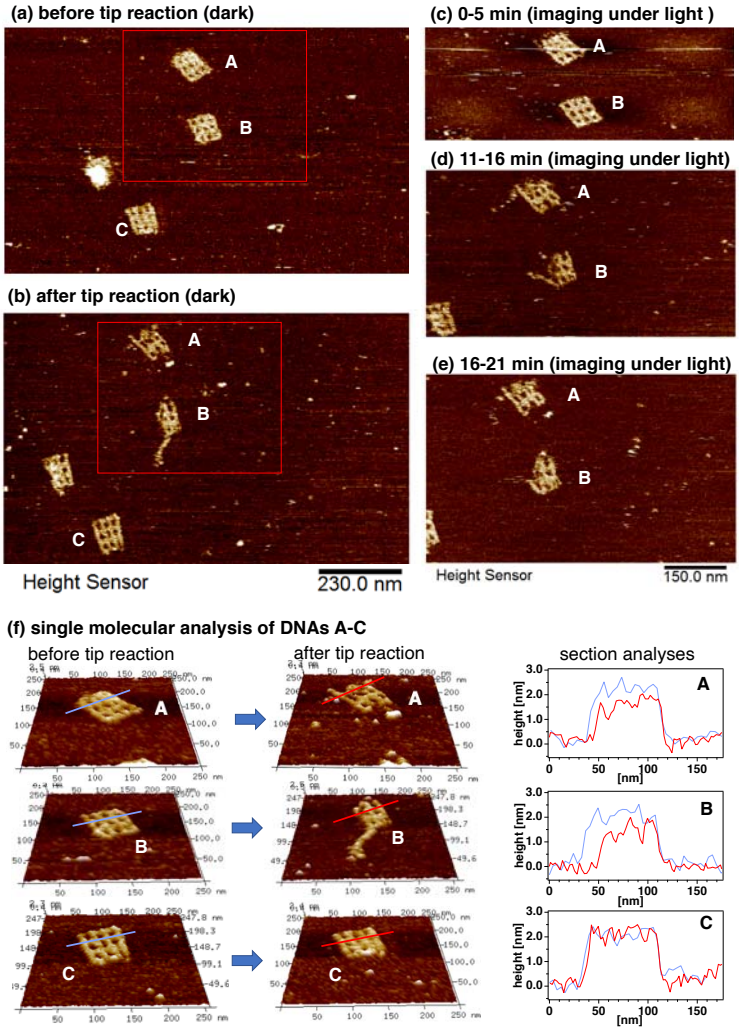

Fig. 5. Single-molecule damage of DNA origami by a chemically functionalized AFM tip with tripod-C_{60} (1) under photoirradiation. (a-b) AFM imaging of a DNA origami substrate over a larger area before (a) and after (b) scanning with tripod-C_{60} AFM tip. The red square indicates the scanned area under photoirradiation. (c-e) AFM images acquired upon scanning with C_{60}-functionalized AFM tip under photoirradiation for 0 – 5 (c), 11 – 16 (d), and 16 – 21 min (e). (f) Single-molecule 3D images and section analyses of treated DNAs **A** and **B**, and control untreated DNA **C**.

It is likely that the observed DNA damage occurred as a consequence of reactive-oxygen species (ROS), especially singlet oxygen ($^1O_2$), generated from the photoexcited C_{60} attached onto the AFM tip surface. In a separate solution-phase experiment, photoinduced $^1O_2$ generation from tripod-C_{60} **1** was clearly observed by trapping with anthracene (Fig. S21). To confirm that the $^1O_2$ is also acting as a reactive species in the tip-induced oxidation reaction, an experiment was carried out in D_2O buffer, where the lifetime of $^1O_2$ is longer in comparison to that in H_2O(*46*), and the DNA damage on the surface are expected to be more dramatic. As shown in Fig. 6, time-lapse imaging revealed that DNA damage by the tripod-C_{60} AFM tip were much faster in D_2O within the scanned area (red square). This result supported the hypothesis that $^1O_2$ is acting as a reactive species involved in tripod-C_{60} tip-based DNA oxidative damage. The involvement of $^1O_2$ was further confirmed by an experiment in the presence of a $^1O_2$ quencher (L-

histidine), which does not show any significant DNA damage by the AFM tip with tripod-C_{60} under photoirradiation for 51 min (Fig. S34).

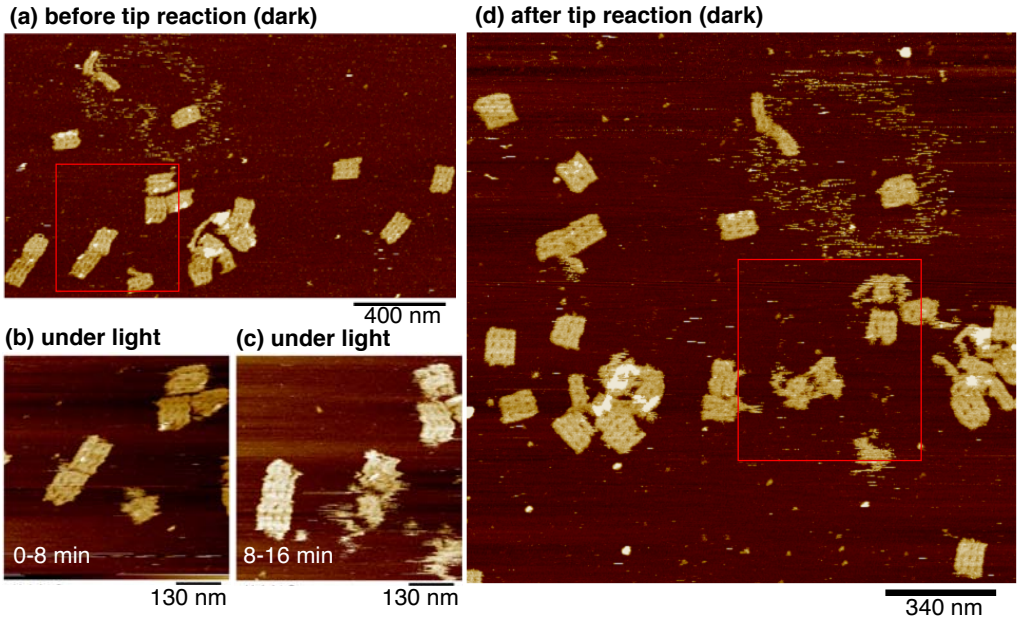

Fig. 6. AFM images for morphology changes of waffle-type DNA origami scanned with a tripod-C_{60} AFM tip under photoirradiation in D_2O. (a) AFM images of a larger area before tip reaction. (b-c) AFM images of a smaller area during the tip reaction with tripod-C_{60} (**1**) tip under photoirradiation for 0 – 8 min (b) and 8 – 16 min (c). (d) AFM images of a larger area after tip reaction. The red squares in (a) and (d) are areas scanned with the tripod-C_{60} (**1**) tip under photoirradiation.

In conclusion, single-molecule oxidative damage of DNA origami was achieved by a chemically functionalized AFM tip bearing a photocatalyst for the localized generation of $^1O_2$. A C_{60} derivative with a rigid tripod scaffold was stably immobilized on a gold-coated AFM tip *via* reaction of disulfides and used to scan the substrate DNA origami. Upon visible-light irradiation, clear morphological changes of the DNA origami, corresponding to their oxidative damage, were observed by AFM imaging, at sites where $^1O_2$ had been generated locally from the C_{60} moiety on the AFM tip. The damage was performed and imaged at a single-molecule level on the nm-scale under tight control of $^1O_2$ generation.

References and Notes:

1. J. Uppenbrink, D. Clery, Single molecules - Introduction. *Science* **283**, 1667-1667 (1999).
2. J. K. Gimzewski *et al.*, Rotation of a single molecule within a supramolecular bearing. *Science* **281**, 531-533 (1998).
3. A. Engel, D. J. Muller, Observing single biomolecules at work with the atomic force microscope. *Nat. Struct. Biol.* **7**, 715-718 (2000).
4. D. G. de Oteyza *et al.*, Direct Imaging of Covalent Bond Structure in Single-Molecule Chemical Reactions. *Science* **340**, 1434-1437 (2013).
5. G. Binnig, C. Gerber, E. Stoll, T. R. Albrecht, C. F. Quate, Atomic Resolution with Atomic Force Microscope. *Europhys. Lett.* **3**, 1281-1286 (1987).

6. C. D. Frisbie, L. F. Rozsnyai, A. Noy, M. S. Wrighton, C. M. Lieber, Functional-Group Imaging by Chemical Force Microscopy. *Science* **265**, 2071-2074 (1994).
7. S. Allen *et al.*, In situ observation of streptavidin-biotin binding on an immunoassay well surface using an atomic force microscope. *FEBS Lett.* **390**, 161-164 (1996).
8. C. B. Yuan, A. Chen, P. Kolb, V. T. Moy, Energy landscape of streptavidin-biotin complexes measured by atomic force microscopy. *Biochem.* **39**, 10219-10223 (2000).
9. Y. Harada, M. Kuroda, A. Ishida, Specific and quantized antigen-antibody interaction measured by atomic force microscopy. *Langmuir* **16**, 708-715 (2000).
10. M. Rief, M. Gautel, F. Oesterhelt, J. M. Fernandez, H. E. Gaub, Reversible unfolding of individual titin immunoglobulin domains by AFM. *Science* **276**, 1109-1112 (1997).
11. T. E. Fisher, P. E. Marszalek, J. M. Fernandez, Stretching single molecules into novel conformations using the atomic force microscope. *Nat. Struct. Biol.* **7**, 719-724 (2000).
12. A. F. Oberhauser, M. Carrion-Vazquez, Mechanical biochemistry of proteins one molecule at a time. *J. Biol. Chem.* **283**, 6617-6621 (2008).
13. R. McKendry, M. E. Theoclitou, T. Rayment, C. Abell, Chiral discrimination by chemical force microscopy. *Nature* **391**, 566-568 (1998).
14. H. Schonherr *et al.*, Individual supramolecular host-guest interactions studied by dynamic single molecule force spectroscopy. *J. Am. Chem. Soc.* **122**, 4963-4967 (2000).
15. T. Auletta *et al.*, beta-cyclodextrin host-guest complexes probed under thermodynamic equilibrium: Thermodynamics and AFM force spectroscopy. *J. Am. Chem. Soc.* **126**, 1577-1584 (2004).
16. S. Kado, K. Kimura, Single complexation force of 18-crown-6 with ammonium ion evaluated by atomic force microscopy. *J. Am. Chem. Soc.* **125**, 4560-4564 (2003).
17. R. D. Piner, J. Zhu, F. Xu, S. H. Hong, C. A. Mirkin, "Dip-pen" nanolithography. *Science* **283**, 661-663 (1999).
18. M. Peter, X. M. Li, J. Huskens, D. N. Reinhoudt, Catalytic probe lithography: Catalyst-functionalized scanning probes as nanopens for nanofabrication on self-assembled monolayers. *J. Am. Chem. Soc.* **126**, 11684-11690 (2004).
19. W. F. Paxton, J. M. Spruell, J. F. Stoddart, Heterogeneous Catalysis of a Copper-Coated Atomic Force Microscopy Tip for Direct-Write Click Chemistry. *J. Am. Chem. Soc.* **131**, 6692-6694 (2009).
20. D. A. Unruh, C. Mauldin, S. J. Pastine, M. Rolandi, J. M. J. Frechet, Bifunctional Patterning of Mixed Monolayer Surfaces Using Scanning Probe Lithography for Multiplexed Directed Assembly. *J. Am. Chem. Soc.* **132**, 6890-6891 (2010).
21. A. R. Sulkanen *et al.*, Spatially Selective and Density-Controlled Activation of Interfacial Mechanophores. *J. Am. Chem. Soc.* **141**, 4080-4085 (2019).
22. E. Dulkeith *et al.*, Fluorescence quenching of dye molecules near gold nanoparticles: Radiative and nonradiative effects. *Phys. Rev. Lett.* **89**, 203002 (2002).
23. Q. Li, A. V. Rukavishnikov, P. A. Petukhov, T. O. Zaikova, J. F. W. Keana, Nanoscale 1,3,5,7-tetrasubstituted adamantanes and p-substituted tetraphenyl-methanes for AFM applications. *Org. Lett.* **4**, 3631-3634 (2002).
24. M. E. Drew, A. Chworos, E. Oroudjev, H. Hansma, Y. Yamakoshi, A Tripod Molecular Tip for Single Molecule Ligand-Receptor Force Spectroscopy by AFM. *Langmuir* **26**, 7117-7125 (2010).

25. D. Takamatsu, Y. Yamakoshi, K. Fukui, Photoswitching behavior of a novel single molecular tip for noncontact atomic force microscopy designed for chemical identification. *J. Phys. Chem. B* **110**, 1968-1970 (2006).
26. D. Takamatsu, K. Fukui, S. Aroua, Y. Yamakoshi, Photoswitching tripodal single molecular tip for noncontact AFM measurements: synthesis, immobilization, and reversible configurational change on gold surface. *Org. Biomol. Chem.* **8**, 3655-3664 (2010).
27. T. Yamazaki, J. G. Heddle, A. Kuzuya, M. Komiyama, Orthogonal enzyme arrays on a DNA origami scaffold bearing size-tunable wells. *Nanoscale* **6**, 9122-9126 (2014).
28. D. R. Han, S. Pal, Y. Liu, H. Yan, Folding and cutting DNA into reconfigurable topological nanostructures. *Nat. Nanotechnol.* **5**, 712-717 (2010).
29. A. Ray *et al.*, Single-Molecule AFM Study of DNA Damage by $^1O_2$ Generated from Photoexcited C_{60}. *J. Phys. Chem. Lett.* **11**, 7819-7826 (2020).
30. J. H. Scofield, Hartree-Slater Subshell Photoionization Cross-Sections at 1254 and 1487ev. *J. Electron Spectrosc.* **8**, 129-137 (1976).
31. Passiu, C. XPS and DFT Investigation of the Au-S Interface, Ph. D. Thesis of ETH Zurich, 2019 (No. 25777).
32. Slower decrease of frequency by the injection of **1**, in comparison to the case of **2**, was presumably due to the lower solubility of **1** in THF.
33. G. Sauerbrey, Verwendung Von Schwingquarzen Zur Wagung Dunner Schichten Und Zur Mikrowagung. *Z. Phys.* **155**, 206-222 (1959).
34. When tripod-C_{60} is immobilized on Au AFM tip in this uplight orientation, C_{60} moiety will be closer to the reaction substrate to efficiently perform the surface oxidation reaction, while will have certain distance from gold surface, which may quench the excited state of C_{60} by energy transfer.
35. The prepared Au surface was to the further reaction with **1** or **2** either immediately after pareparation or used after clearning by UV-Ozone cleaner preor to use.
36. L. Martinez, L. G. Carrascosa, Y. Huttel, L. M. Lechuga, E. Roman, Influence of the linker type on the Au-S binding properties of thiol and disulfide-modified DNA self-assembly on polycrystalline gold. *Phys. Chem. Chem. Phys.* **12**, 3301-3308 (2010).
37. D. G. Castner, K. Hinds, D. W. Grainger, X-ray photoelectron spectroscopy sulfur 2p study of organic thiol and disulfide binding interactions with gold surfaces. *Langmuir* **12**, 5083-5086 (1996).
38. E. Pensa *et al.*, The Chemistry of the Sulfur-Gold Interface: In Search of a Unified Model. *Acc. Chem. Res.* **45**, 1183-1192 (2012).
39. O. Cavalleri, L. Oliveri, A. Dacca, R. Parodi, R. Rolandi, XPS measurements on L-cysteine and 1-octadecanethiol self-assembled films: a comparative study. *Appl. Surf. Sci.* **175**, 357-362 (2001).
40. J. J. Blackstock, Z. Y. Li, G. Y. Jung, Template stripping using cold welding. *J. Vac. Sci. Technol. A* **22**, 602-605 (2004).
41. D. Takamatsu, K. Fukui, S. Aroua, Y. Yamakoshi, Photoswitching tripodal single molecular tip for noncontact AFM measurements: synthesis, immobilization, and reversible configurational change on gold surface. *Org. Biomol. Chem.* **8**, 3655-3664 (2010).
42. N. Vogel, J. Zieleniecki, I. Koper, As flat as it gets: ultrasmooth surfaces from template-stripping procedures. *Nanoscale* **4**, 3820-3832 (2012).
43. E. A. Weiss *et al.*, Si/SiO_2-Templated formation of ultraflat metal surfaces on glass, polymer, and solder supports: Their use as substrates for self-assembled monolayers. *Langmuir* **23**, 9686-9694 (2007).

44. It is reported that the DNA structures are generally stable under AFM imaging condition with a force of <260 nN.
45. Y. Wang *et al.*, Nanomanipulation of Individual DNA Molecules Covered by Single-Layered Reduced Graphene Oxide Sheets on a Solid Substrate. *J. Phys. Chem. B* **122**, 612-617 (2018).
46. B. A. Lindig, M. A. J. Rodgers, A. P. Schaap, Determination of the Lifetime of Singlet Oxygen in D_2O Using 9,10-Anthracenedipropionic Acid, a Water-Soluble Probe. *J. Am. Chem. Soc.* **102**, 5590-5593 (1980).
47. J. L. Hutter, J. Bechhoefer, Calibration of Atomic Force Microscope Tips. *Rev. Sci. Intrum.* **64**, 1868-1873 (1993).

Acknowledgments

Funding: Supported by SNF project grant 200021_156097 (Y.Y.) and ETH grant ETH-45 19-1 (Y.Y.). **Author contributions:** A.Ray., C.P. and M.N. are the primary experimentalists. A.Ray. performed synthesis of tripods, C.P. performed XPS analysis, and A.Ray. performed other surface analyses and AFM imaging. A.Rossi, S.R. and N.D.S supervised surface analyses and AFM imaging. A.K. designed and synthesized DNA origami. Y.Y. led the team and designed the experiment and analysis. Y.Y., A.R., C.P. and N.D.S wrote and edited the manuscript. **Competing interests:** Authors declare no competing interests. **Data and materials availability:** The supplementary materials contain complete experimental spectral details for all new compounds and surface characterization data reported herein.

Supplementary Materials:

Materials and Methods

Figures S1-S34

Tables S1-S3
References (*23, 24, 31, 33, 42, 43*)